

1 Estimating mineral aerosol iron and aluminum
2 solubility from particle size using diffusion-controlled
3 and surface-area-controlled approximations

Qin Han,¹ Charles S. Zender,¹ J. Keith Moore,¹ Clifton S. Buck,² Ying
Chen,³ Anne Johansen,⁴ and Christopher I. Measures⁵

¹Department of Earth System Science,
University of California, Irvine, California,
USA.

²Department of Oceanography, Florida
State University, Tallahassee, Florida, USA.

³Department of Environmental Science
and Engineering, Fudan University,
Shanghai, P.R. China

⁴Chemistry Department, Central
Washington University, Ellensburg,
Washington, USA

⁵Department of Oceanography, University
of Hawai'i at Manoa, Honolulu, Hawaii,
USA

4 **Abstract.** Mineral aerosol deposition is recognized as the dominant source
5 of iron to the open ocean and the solubility of iron in the dust aerosol is highly
6 variable, with measurements ranging from 0.01-80%. Global models have dif-
7 ficulty capturing the observed variations in solubility, and have ignored the
8 solubility dependence on aerosol size. We introduce two idealized physical
9 models to estimate the size dependence of mineral aerosol solubility: a diffusion-
10 controlled model and a surface-area-controlled model. These models produce
11 differing time and spatial varying solubility maps for aerosol Fe and Al given
12 the dust age at deposition, size-resolved dust entrainment fields, and the aerosol
13 acidity. The resulting soluble iron deposition fluxes are substantially differ-
14 ent, and more realistic, than a globally uniform solubility approximation. The
15 surface-area-controlled solubility varies more than the diffusion-controlled
16 solubility and better captures the spatial pattern of observed solubility in
17 the Atlantic. However, neither of these two models explains the large solu-
18 bility variation observed in the Pacific. We then examine the impacts of spa-
19 tially variable, size-dependent solubility on marine biogeochemistry with the
20 Biogeochemical Elemental Cycling (BEC) ocean model by comparing the mod-
21 eled surface ocean dissolved Fe and Al with observations. The diffusion-based
22 variable solubility does not significantly improve the simulation of dissolved
23 Fe relative to a 5% globally uniform solubility, while the surface-area-based
24 variable solubility improves the simulation in the North Atlantic but wors-
25 ens it in the Pacific and Indian Oceans.

1. Introduction

26 Iron is a critical nutrient for organisms in the ocean and thus has an important impact
27 on the ocean biogeochemical cycles and the global carbon cycle. Iron deficiency limits the
28 primary production in High-Nutrient Low-Chlorophyll (HNLC) ocean regions [*Martin*
29 *and Fitzwater*, 1988; *Behrenfeld et al.*, 1996; *Boyd et al.*, 2000]. In the remote oceans,
30 atmospheric transport and deposition is a key source of iron to the surface waters [*Fung*
31 *et al.*, 2000; *Jickells and Spokes*, 2001]. Numerous modeling and experimental studies
32 have investigated the concentration, deposition and solubility of atmospheric aerosols.
33 However, the bio-available iron deposition is still not well known and more studies on
34 aerosol iron solubility are required [*Jickells et al.*, 2005].

35 Aluminum, on the other hand, is not found to be an important nutrient but is a useful
36 tracer for crustal material [*Arimoto et al.*, 2003]. However, due to its special geochemical
37 characteristics, e.g. common and relatively invariant content ($\sim 8\%$) over the Earth's crust
38 [*Wedepohl*, 1995], relatively short residence time (~ 6.5 yr) in the surface ocean [*Jickells*
39 *et al.*, 1994] and relatively simple chemistry compared to Fe, aluminum has been used as a
40 tracer for quantifying the dust deposition to the surface ocean [*Measures and Vink*, 2000;
41 *Han et al.*, 2008]. *Han et al.* [2008] ignored the spatial variation of mineral dust solubility
42 and treated Al solubility as size-independent.

43 Iron in mineral dust is not very soluble ($\sim 0.5\%$) in source regions [*Fung et al.*, 2000] and
44 usually becomes more soluble by the time of deposition. The reported atmospheric iron
45 solubility spans over three orders of magnitude (0.01%–80%) [*Mahowald et al.*, 2005]. *Shi*
46 *et al.* [2010] simulated acid processes in the atmosphere and measured the potential Fe

47 solubility of dust precursor samples from North African dust source regions to vary from
48 0.7% to 17.3%. Fewer Al solubility measurements are available but existing data also show
49 strong spatial variations (0.5%-86%) [*Prospero et al.*, 1987; *Baker and Jickells*, 2006; *Buck*
50 *et al.*, 2006, 2008b; *Measures et al.*, 2010]. Atmospheric processes seem to increase mineral
51 aerosol iron solubility during transport from source regions to the open oceans [*Jickells and*
52 *Spokes*, 2001; *Mahowald et al.*, 2005]. Several solubilizing mechanisms have been proposed
53 including processing by natural and anthropogenic organic acids [*Zuo and Holgné*, 1992;
54 *Siefert et al.*, 1994] and by sulfate and nitrate coatings [*Zhuang et al.*, 1992; *Zhu et al.*,
55 1992] that, along with photochemical processing, occurs both within and outside of clouds
56 [*Jickells and Spokes*, 2001; *Hand et al.*, 2004; *Johansen and Key*, 2006]. It has also
57 been proposed that soluble iron has large combustion sources including biomass burning
58 [*Chen and Siefert*, 2004; *Chuang et al.*, 2005] and combustion of heavy fuel oil [*Sholkovitz*
59 *et al.*, 2009]. There is evidence that mineralogical changes in Fe speciation (e.g., due to
60 combustion) are important in determining solubility [*Shi et al.*, 2009, 2011]. *Sholkovitz*
61 *et al.* [2009] also discussed the physical mixing of chemically distinct aerosol populations
62 at Bermuda and the affect on observations of aerosol iron solubility. Unfortunately, global
63 models based on these mechanisms have difficulty predicting the observed solubility [*Hand*
64 *et al.*, 2004; *Luo et al.*, 2005; *Fan et al.*, 2006; *Luo et al.*, 2008].

65 *Baker and Jickells* [2006] argue that the control of Fe solubility is primarily physical
66 rather than chemical in nature. They find a positive correlation between solubility and the
67 surface area to volume ratio of dust particles. Observations show enrichment of labile Fe
68 in fine aerosol samples compared to coarse aerosols [*Siefert et al.*, 1999; *Johansen et al.*,
69 2000; *Chen and Siefert*, 2004]. On the other hand, *Hand et al.* [2004] suggested that

70 the prolonged acid and photochemical processing of fine particles could be responsible
71 for their higher Fe solubility relative to larger particles which have a shorter atmospheric
72 lifetime. Thus the globally uniform, size-independent, constant Al solubility used by *Han*
73 *et al.* [2008] is unrealistic and may contribute to the model-observation discrepancies.

74 In this work, we develop two distinct conceptual models of mineral aerosol solubility
75 based on diffusion-controlled dissolution and surface-area-controlled dissolution, respec-
76 tively. These models estimate solubility as a function of particle size, atmospheric trans-
77 port time, and aerosol acidity. Using the particle size distribution, acid deposition flux
78 and aerosol age predicted by global models, we produce two global solubility maps and
79 apply them to an ocean ecosystem model. The model results allow us to evaluate the sim-
80 ulated sensitivity of aerosol solubility to particle size, and to test each conceptual model
81 for advantages in simulating the observed distribution of dissolved Fe and Al.

2. Methods

2.1. Conceptual model I: classical diffusion-controlled dissolution

82 Chemical diffusion occurs when there is a gradient in chemical potential, which is gen-
83 erally described by Fick's first law. In solid-Earth systems, several diffusion pathways
84 exist in rocks as well as in individual mineral grains. The diffusivity of mineral grains
85 may depend upon the presence of fast pathways—extended defects in the crystal lattice,
86 which are migrations along extended intracrystalline defects such as dislocations. Water
87 condenses to a particle's surface soon after it encounters air with relative humidity (RH)
88 $\geq 20\%$ [*Grassian*, 2001]. The dissolution of dust particles begins immediately on contact
89 with a liquid coating like water. From the view of classical diffusion theory, the dissolution
90 process consists of four steps: (1) diffusion of species A (in this study, A can be Fe or

Al) inside the “solid” particle from center to surface; (2) transfer of the species across the interface; (3) aqueous dissociation reaction; (4) diffusion of species A from the interface. The diffusion-like process we envision taking place within mineral dust particles is dominated by relatively fast leaching of trace species through the fissures, imperfections, and cracks of aspherical dust aggregates [Anderson *et al.*, 1996]. Since the characteristic time of step 1 is 6 or more orders of magnitude longer than other steps, the solubility of species A is controlled mainly by step 1.

2.1.1. Solving the diffusion equations

Based on Fick’s Second Law, we describe step 1 mathematically

$$\frac{\partial N_A}{\partial t} = D_A \left(\frac{\partial^2 N_A}{\partial r^2} + \frac{2}{r} \frac{\partial N_A}{\partial r} \right) \quad (1)$$

with the following initial and boundary conditions:

$$N_A(r, 0) = N_0, \quad r < R_p \quad (2)$$

$$N_A(R_p, t) = N_S \quad (3)$$

$$\left(\frac{\partial N_A}{\partial t} \right)_{r=0} = 0 \quad (4)$$

$N_A(r, t)$ is the concentration of species A; R_p is the radius of the particle; N_0 is the initial concentration; N_S is the concentration of A at the particle’s surface; D_A is the diffusion coefficient.

Following *Seinfeld and Pandis* [2006], we solve the diffusion equation and get the maximum solubility of species A at time t :

$$\begin{aligned} S^{\max} &= \int_0^t J_c^{\max} \\ &= \frac{6}{\pi^2} \sum_{n=1}^{\infty} \frac{1}{n^2} \left[1 - \exp \left(-\frac{n^2 \pi^2 D_A t}{R_p^2} \right) \right] \end{aligned} \quad (5)$$

106 $J_c^{\max}(R_p, t)$ is the diffusive flux of A outward at the particle surface assuming the concen-
 107 tration of A at the particle surface vanishes ($N_S = 0$), as it does for freshly condensed
 108 liquid aerosols that coat mineral dust when $RH \geq 20\%$. This assumption is relaxed in the
 109 next section.

110 **2.1.2. Constraining the solubility with available condensed water**

111 Equation (5) does not limit dissolution of species A so $S^{\max} \rightarrow 100\%$ after a long time.
 112 This is unrealistic because the dissolution rate will decrease as the trace concentration
 113 in the solution coating the dust increases. An equilibrium between the solution and the
 114 particle results when the dissolution rate reduces to zero before the particulate species A
 115 completely dissolves.

116 *Hänel* [1976] gives an empirical relationship between the increased particle radius after
 117 the hygroscopic growth and the relative humidity:

$$r_g \approx r \times (1 - RH)^{-\epsilon} \quad (6)$$

118 r_g is the radius of the particle after hygroscopic growth; r is the original radius of the
 119 particle; RH is the relative humidity of the ambient air; ϵ is the experimental coefficient
 120 varies with the category of the aerosols. Here we use $\epsilon = 0.18$ for dust in the Atlantic
 121 marine environment [*Hänel*, 1976]. Thus with an atmospheric relative humidity of 80%,
 122 condensed water increases the original particle's volume by 140% and this limits the
 123 maximum solubility to 70%.

124 **2.1.3. Determining the diffusion coefficient**

125 Diffusion coefficients for different geologic materials vary broadly and are largely de-
 126 pendent on temperature and pressure. *Watson and Baxter* [2007] show that the diffu-

127 sion coefficient in minerals range from $D_A \approx 10^{-20} \text{ m}^2 \text{ s}^{-1}$ to $10^{-50} \text{ m}^2 \text{ s}^{-1}$ at $500 \text{ }^\circ\text{C}$,
 128 and typically lower at normal atmospheric temperature and pressure conditions. In our
 129 diffusion-controlled solubility model, only diffusion coefficients D_A near $10^{-22} \text{ m}^2 \text{ s}^{-1}$ yield
 130 the measured range of dust solubilities within the average dust particle lifetime in the at-
 131 mosphere of ~ 4 days (Figure 1). We use $D_A = 1.2 \times 10^{-22} \text{ m}^2 \text{ s}^{-1}$ which best simulates
 132 the observed solubilities.

2.2. Conceptual model II: surface-area-controlled dissolution

133 The second conceptual model considers the aerosol solubility to be controlled by the
 134 exposed surface area of the dust particle and neglects any diffusive processes inside the
 135 mineral dust particles. The dissolution rate f [mol s^{-1}] is determined by the detachment
 136 rate of reaction k [$\text{mol m}^{-2} \text{ s}^{-1}$] acting over the total surface area A [m^2] [Stumm, 1992]:

$$f = k \times A \quad (7)$$

137 Here k varies with species, pH, and temperature. For complex particles and aggregates
 138 like mineral dust, A depends on the surface roughness factor λ and the geometric surface
 139 area $s(r)$ [m^2] as:

$$A = \lambda \times s(r) \quad (8)$$

140 Thus for any particle, the fractional solubility S is:

$$S(r, t) = \frac{M \times k \times \lambda \times s(r) \times t}{V(r) \times \rho \times C_1} \quad (9)$$

141 M is the molar mass of Fe [$55.845 \text{ g mol}^{-1}$] or Al [$26.982 \text{ g mol}^{-1}$]; t is the elapsed time of
 142 dissolution (taken here to be the atmospheric transport time); $V(r)$ is the particle volume

143 $[\text{m}^3]$; $\rho = 2.5 \times 10^6 \text{ g m}^{-3}$ is the density of dust particles and $C_1 = 3.5\%$ is the assumed
144 iron content in dust [*Taylor and McLennan, 1985*].

145 **2.2.1. Choosing the parameters**

146 During the last few decades, intensive research has been done on the mineral-water-
147 surface-controlled dissolution process and the specified reaction rate k has been measured
148 through both laboratory work and natural system studies for many kinds of minerals
149 under various conditions [*Stumm, 1992; Brantley, 2008*]. The reaction rates of various
150 Al-minerals range from 1.5×10^{-10} to $2.0 \times 10^{-13} \text{ M m}^2 \text{ s}^{-1}$ at 25° and $\text{pH} = 3$ [*Wehrli*
151 *et al., 1990*]. Goethite/hematite are thought to be dominant Fe reservoirs in mineral dust
152 [*Claquin et al., 1999; Lafon et al., 2006*]. Other iron-containing aluminosilicates, such
153 as clay, contribute to soluble iron as well [*Journet et al., 2008*]. For laboratory-ground
154 goethite and hematite particles, an empirical relationship between the reaction rates and
155 pH is found to be $\log(k) = -10.98 - 0.43 \times \text{pH}$ [*Cheah et al., 2003; Brantley et al., 2006*].
156 Although this relation is based on only goethite and hematite, it produces solubilities in
157 agreement with observations of ambient dust if we increase k yet retain its pH -dependence
158 by altering the relation to:

$$\log(k) = -10.13 - 0.43 \times \text{pH} \quad (10)$$

159 Since no measured relation between the detachment rate k or the dissolution rate f and
160 pH has been reported for Al, we also use Equation (10) for Al. The soluble Al deposition
161 flux will be calculated using Fe solubility and 8% Al content in dust.

162 The pH values were measured before dissolution in the empirical relationship (10). What
163 complicates the application of (10) in global models is that aerosol pH evolves continually

164 due to aerosol solubilisation [*Desboeufs et al.*, 2003] and to spatio-temporarily varying
 165 aerosol emissions and removal processes. Several cruises have found a positive correlation
 166 between solubility and the ratio of aerosol acids to dust mass [*Sato*, 2003; *Chen and*
 167 *Siefert*, 2004]. We approximate the acidity of dust coatings during transport using the
 168 valence-adjusted ratios of sulfate and nitrate aerosol fluxes to dust flux at deposition:

$$pH^* = -\log \left(\frac{F_{\text{SO}_4^{2-}} \times 2 + F_{\text{NO}_3^-}}{F_{\text{dust}}^{\frac{1}{3}} \times C_2} \right) \quad (11)$$

169 $F_{\text{SO}_4^{2-}}$, $F_{\text{NO}_3^-}$ are the annual deposition flux fields for sulfate and nitrate estimated by
 170 *Luo et al.* [2007] using the UC Irvine global chemistry transport model (UCICTM) with
 171 an embedded aerosol equilibrium model; F_{dust} is the climatological dust deposition flux
 172 from driving the Dust Entrainment and Deposition (DEAD) model with NCEP/NCAR
 173 reanalysis for the period 1990-1999 [*Zender et al.*, 2003]; C_2 is a unitless scale factor. Since
 174 the range of dust fluxes is several orders of magnitude wider than the range of acid fluxes,
 175 we use the cubic root of dust fluxes to create a reasonable global pH distribution of the
 176 atmospheric aerosols.

177 The surface roughness factor λ is the BET surface area [*Brunauer et al.*, 1938, BET
 178 consists of the first initials of the authors' family names.] divided by the geometric surface
 179 area $s(r)$. This factor largely depends on the weathering condition, i.e., the age and
 180 aggregation of the bulk soil. It can be as high as 620 for very old soils and less than 10
 181 for new soils [*White et al.*, 1996]. It also depends on the type of soil and tends to increase
 182 with increasing particle size [*Anbeek*, 1992; *White et al.*, 1996]. Most roughness factor
 183 measurements are for particles larger than 10 μm , while we are most interested in long
 184 range transported particles smaller than 10 μm . We pick $\lambda = 100$ for which the computed
 185 particle specific surface areas agree well with laboratory measurements [*Brantley et al.*,

186 2006; *Cwiertny et al.*, 2008; *Journet et al.*, 2008] for the size range (0.1-10.0 μm) modeled
187 here.

188 A potential problem for this method raises when the aerosol particle is strongly acidic
189 (e.g., $\text{pH} < 1$) for a very long period (e.g., on the scale of months). It is possible to
190 get a solubility of larger than 100% following the formulars above under such extreme
191 conditions since there is no buffer terms to reduce the dissolution rate. One possible way
192 to eliminate this problem is to compare the concentration of Fe or Al in the solution (the
193 liquid coating surrounding the particle) to the measured chemical activities of Al^{3+} , Fe^{3+}
194 in water equilibrium extracts from acid mine drainage [*Sullivan et al.*, 1988; *Sposito*, 1996;
195 *Ahum and Lavkulich*, 1998]. However, these measurements are for particles of millimeters
196 in size or larger and therefore the measured activities are far less than the normal Fe^{3+}
197 concentration in our calculation. Fortunately, such strong acidic condition rarely exists
198 and 90% of dust deposits less than 10 days since emission [*Han and Zender*, 2010] so that
199 this potential problem has little impact.

2.3. Solubility observations

200 Iron solubility has been measured with different techniques that are not completely
201 mutually consistent and intercomparable. We compiled a database of iron solubility field
202 observations to evaluate our models.

203 Soluble iron measurements were performed from the MP01-MP09 cruises in the Pacific
204 and Atlantic Oceans [*Johansen et al.*, 2000; *Chen and Siefert*, 2004]. Two size fractions
205 (diameter $D < 2.5 \mu\text{m}$ for fine fraction and $D > 2.5 \mu\text{m}$ for coarse fraction) of am-
206 bient aerosol samples were collected using a high-volume dichotomous virtual impactor
207 (HVDVI). Labile Fe(II), labile Fe(III) and reducible particulate Fe were operationally de-

208 fined and measured by the extraction time and reagents. The total iron concentration was
209 analyzed using inductively coupled plasma mass spectrometry after a strong-acid digestion
210 procedure. Previous studies used both Fe(II) and labile Fe(II and III) as soluble iron to
211 compare with model results [*Luo et al.*, 2005, 2008]. In our work, we define iron solubility
212 for these measurements as $[\text{Fe(II)}+\text{Fe(III)}]/(\text{Total Fe})\times 100$ for a better compatibility with
213 other methods.

214 Following *Sarthou et al.* [2003], the aerosol samples from RV Polarstern (ANT18-1),
215 RRS James Clark Ross (JCR) and FS Meteor cruise M55 in the Atlantic Ocean were
216 collected using a high volume sampler ($1\text{ m}^3/\text{min}$) and then separated to fine/coarse
217 fractions at $D = 1\ \mu\text{m}$ [*Baker et al.*, 2003]. Soluble iron was extracted by leaching the
218 aerosol sample filters in ammonium acetate buffer at $\text{pH} = 4.7$ for 1–2 h. The supernatant
219 was then drawn through a $0.2\ \mu\text{m}$ filter, acidified with HNO_3 and analyzed for total iron.
220 *Luo et al.* [2008] applied a 0.5 factor when comparing Fe(II) to these measurements. In
221 contrast, we compare to the unmodified measurements since we use total (Fe(II)+Fe(III))
222 labile iron.

223 The aerosols from A16N CLIVAR cruise in the Atlantic and 2002 IOC cruise in the
224 Pacific were measured as described in *Buck et al.* [2006, 2008a, b]. Aerosol samples
225 were collected by an automatic sector-controlled system at a flow rate of 30-50 L/min.
226 Unlike other techniques, they measured the "instantaneous" soluble Fe and Al by quickly
227 passing 100 mL of filtered surface seawater or unacidified DI water ($\text{pH} = 5.6$) through the
228 aerosol sample filter. These correspond to their seawater soluble iron or DI water soluble
229 iron respectively. The total iron was obtained using energy-dispersive X-ray fluorescence
230 (EDXRF). The DI water solubility is generally higher than the seawater solubility. We

231 find that seawater solubility is more comparable with solubilities observed from other
232 cruises than DI solubility. Solubility data from two new Pacific CLIVAR cruises are also
233 included in our database.

234 Al solubility data are only available on cruises 2002 IOC and the Atlantic and Pacific
235 CLIVAR for DI water and on cruise JCR. Hence we focus on comparing iron solubility in
236 this work. We use the solubility in seawater from the CLIVAR and IOC cruises to constrain
237 the parameters (D_A and k) in our conceptual models, and then we compare our model
238 results with the remaining observations. Although these observations were made using
239 different approaches for measuring solubility, they all share the common characteristic
240 that they are based on a simple leaching solution not subject to iron solubility constraints
241 [*Baker and Croot, 2010*].

2.4. Models

242 In this work, we use the monthly mean dust deposition field obtained from driving
243 the Dust Entrainment And Deposition (DEAD) model with 1990s observed meteorology
244 [*Zender et al., 2003; Mahowald et al., 1997*]. The DEAD model simulates size dependent
245 dust processes including mobilization, transport, and dry and wet deposition for particles
246 size from 0.1–10 μm which includes most long-range transported dust. These particles
247 are put into four size bins (0.1–1.0, 1.0–2.5, 2.5–5.0, 5.0–10.0 μm) and are assumed to be
248 log-normally distributed within each bin [*Zender et al., 2003*].

249 We will compare the response of the Biogeochemical Elemental Cycling (BEC) ocean
250 model [*Moore et al., 2004*] with soluble Fe and Al fluxes from our spatially variable solu-
251 bility models to the ecosystem response to the constant 5% solubility (the base run) used
252 before [*Han et al., 2008*]. The BEC ocean model couples the upper ocean ecosystem model

253 [*Moore et al.*, 2002] and an expanded biogeochemistry module [*Doney et al.*, 2003] with the
254 ocean circulation component of the Community Climate System Model 3.0 [*Collins et al.*,
255 2006]. This marine ecosystem model includes one zooplankton and four phytoplankton
256 functional groups: coccolithophores, small phytoplankton, diatoms, and diazotrophs; key
257 limiting nutrients: nitrate, ammonium, phosphate, iron, and silicate; sinking particulates
258 and dissolved organic matter. In these components, the model tracks carbon, nitrogen,
259 phosphorus, iron, silicon, oxygen and calcium carbonate and then predicts the biomass,
260 productivity, community structure, and carbon export in the ocean ecosystem. Al cycling
261 has been incorporated into the BEC model [*Han et al.*, 2008]. In addition, the version
262 used here includes improvements in the iron scavenging parameterizations and the more
263 realistic sedimentary iron source from *Moore and Braucher* [2008]. We optimized the Fe
264 and Al scavenging coefficients for each soluble Fe and Al deposition map with all other pa-
265 rameter values staying identical in the three simulations. The observations of dissolved Fe
266 and Al concentrations in the surface ocean have been summarized by *Moore and Braucher*
267 [2008] and *Han et al.* [2008] respectively.

3. Results

3.1. Modeled solubility for variable particle sizes

268 The predicted solubility increases with time for both conceptual models (Figure 2a-c)
269 and smaller particles (size bins 1 and 2, $0.1 < D < 2.5 \mu\text{m}$) always have higher solubilities
270 than larger particles. Initially, the diffusion-controlled model and the surface-controlled
271 model at $\text{pH} = 3$ predict similar solubilities. After ~ 10 days the model solubility predic-
272 tions diverge. The solubility predicted by the diffusion-controlled model levels off with
273 time due to the limited condensed water (i.e., particle coating) available. The maximum

274 solubility predicted from the diffusion-controlled model is $\sim 70\%$. The solubility predicted
275 by the surface-area-controlled model increases linearly with time and reaches the maxi-
276 mum of 100% in ~ 60 days for the sub-micron dust (size bin 1) with coatings at pH = 3.
277 This maximum is rarely reached during transport since 90% of dust deposits within 10
278 days since emission [*Han and Zender, 2010*].

279 Iron dissolves much faster at lower pH in the surface-controlled model. At a fixed time
280 $t = 4$ days (which is the mean dust residence time in the atmosphere), the particle is
281 almost non-soluble at pH > 4 and solubility increases exponentially as pH decreases from
282 4 (Figure 2d). It takes ~ 10 days at pH = 3 to reach 2–15% solubility and only 30 hours
283 at pH = 1. This is consistent with the laboratory measurements of iron solubility ranging
284 from 6–17% for different dust source samples at pH = 1 after 30 hours [*Cwiertny et al.,*
285 2008].

3.2. Geographic distribution of solubility

286 With size-resolved geographic dust deposition fluxes from DEAD [*Zender et al., 2003*]
287 and dust age at deposition from MAT [*Han and Zender, 2010*], we estimated the Fe or Al
288 solubility in deposited dust at any location from the relation (5) between solubility, dust
289 size and transport time, based on the diffusion-controlled conceptual model (Figure 3a).
290 Using the climatological pH distribution estimated in *Luo et al. [2007]*, we estimated the
291 distribution of Fe solubility based on the surface-controlled conceptual model (Figure 3b).
292 Both solubility maps show very low solubility over the continents near dust source regions
293 such as Northern Africa, Australia and central Asia, as well as over oceanic regions down-
294 wind from dust sources such as the northern equatorial Atlantic. Both models estimate
295 the lowest solubilities, under 0.5%, in deserts. Solubilities outside the dust source regions

296 depend sensitively on the conceptual model, though all solubilities increase with trans-
297 port time and with smaller particle sizes. All solubilities are low near to and downwind
298 from source regions where the large particles are still abundant and the dust is young.
299 Solubilities increase farther from source regions.

300 The highest diffusion-based solubilities (Figure 3a) occur in the equatorial Pacific where
301 the deposited dust age is very old (~ 30 days) and small dust particles dominate. Diffusion-
302 based solubilities over most of the Atlantic are lower than 6% except the area from 5–30 °S
303 and in the far northwest. Solubilities over the Pacific are generally higher than 6% except
304 downwind from Australian, North American, and East Asian sources. Solubilities over
305 the Southern Ocean range from 1% to 10% depending on the proximity of the area to
306 dust source regions.

307 The solubility distribution estimated from the surface-area-controlled model (Figure 3b)
308 is largely controlled by the estimated aerosol acidity, i.e., by the relative abundance of
309 acids (sulfate and nitrate) to dust rather than the dust particle size and dust age at depo-
310 sition. Solubility in and near source regions is still low due to the high dust concentration
311 and the young dust age. But the highest solubilities occur where the estimated acid depo-
312 sition fluxes are highest relative to dust deposition fluxes, e.g. southeastern Asia, western
313 Europe, eastern North America and northern South America. The highest solubilities ex-
314 ceed 40%, more than twice the highest estimated solubilities from the diffusion-controlled
315 model. The solubilities over most ocean areas range from 4–10% due to the moderate
316 acid to dust ratio and the moderate dust age. Exceptions include the northern equatorial
317 Atlantic and 0–70 °W of the Southern Ocean where modeled solubilities are very low (less
318 than 2%) due to being downwind of strong dust and weak pollution sources. There is only

319 one observation near the Southern Ocean (at 52 °W 43 °S where solubility was measured
320 as 4.21%) so it is difficult to assess whether the low modeled solubilities are observed in
321 this important Fe-limited region. The modeled solubility over the northwestern Pacific
322 exceeds 10% due to the strong pollution sources upwind. Dust solubility is quite low over
323 pristine remote regions such as Antarctica.

3.3. Model-data comparisons

324 The parameters (i.e., D_A and k) that were constrained by the cruises IOC and CLIVAR
325 data produce widely scattered solubilities compared to observations from other cruises
326 (Figure 4). The diffusion-controlled model does not fit the cruise data well over the
327 Atlantic Ocean ($R = 0.07$). Most simulated solubilities are within a factor of two of
328 the corresponding observations, and are too high where the observed solubilities are less
329 than 3%. The surface-controlled model simulates, on average, lower solubilities than the
330 diffusion-controlled model. This model underestimates many points yet it captures the
331 overall solubility pattern over the Atlantic ($R = 0.57$, significant at the 95% level). How-
332 ever, neither model captures the spatial solubility pattern over the Pacific (insignificant
333 correlations of $R = -0.04$ and 0.13). Observed solubilities range from less than 1% to
334 more than 20% across the Pacific, while our model predictions range only from 3%–10%
335 at the same locations. An important reason for this model-data misfit in solubility could
336 be the neglect of anthropogenic iron in our model, especially for the Pacific Ocean where
337 the natural dust deposition is low and thus the anthropogenic source of soluble Fe is rela-
338 tively more important. Neglecting anthropogenic iron may also explain the underestimate
339 of solubility from the surface-controlled model over the Atlantic Ocean.

3.4. Soluble iron deposition maps

340 The two models predict similar total depositions of soluble iron to oceans (0.47-0.48
341 Tg/yr), and are close to the total soluble Fe (0.57 Tg/yr) deposited from a globally uniform
342 solubility assumption of 5%. However, the distributions within ocean basins differ greatly
343 (Figure 5, Table 1). Both size-resolving solubility models predict higher (relative and
344 absolute) soluble Fe fluxes to the Pacific and South Atlantic than the globally uniform
345 solubility assumption, and lower fluxes to other oceans. The three factors responsible
346 for this pattern are: (1) the long transit times, (2) preferential survival of small particles
347 during transport and (3) generally high pollution-to-dust ratios on a basin-wide scale
348 for the Pacific and South Atlantic Ocean. The diffusion-controlled model budget, when
349 evaluated regionally, is closer than the surface-controlled model budget to the 5% solubility
350 budget. The surface-controlled model predicts twice the soluble iron flux to the Pacific
351 and 40% more to the South Atlantic than the 5% assumption. The soluble iron flux
352 from the surface-controlled model is much smaller in the equatorial Atlantic than a 5%
353 solubility flux, yet is only 20% less when averaged over the entire North Atlantic. The
354 most dramatic difference occurs in the Southern Ocean where the surface-controlled model
355 predicts only 15% of the soluble iron flux as the 5% solubility assumption—equivalent to
356 a solubility of only 0.7%. This result is speculative since there are no direct iron solubility
357 measurements in the Southern Ocean for comparison.

358 The soluble Fe deposition maps from this study are similar to previous global stud-
359 ies that neglect explicit particle-size dependent processes on solubility [*Luo et al.*, 2008;
360 *Mahowald et al.*, 2009]. This is not surprising since the dust deposition fields in these
361 studies are predicted with similar physics and agree over many orders of magnitude. The

362 global total (land+ocean) soluble iron depositions from these studies are also comparable
363 (0.90-0.98 Tg/yr here, 0.89 Tg/yr in *Luo et al.* [2008]). However, this study predicts more
364 than twice the soluble iron deposition to oceans than *Luo et al.* [2008] but only 1/5 of *Fan*
365 *et al.* [2006]. The study also nearly quadruples the soluble iron deposition to the North
366 Atlantic in *Luo et al.* [2008]. Though our surface-controlled model shows a slightly better
367 correlation in the Atlantic, none of these models stands out as being the most consistent
368 with all available observations.

3.5. Ecosystem model responses to variable solubility

369 Overall, the dissolved Fe and Al concentrations in surface oceans simulated by the
370 BEC model [*Moore and Braucher*, 2008; *Han et al.*, 2008] driven by the variable solu-
371 bility from either our diffusion- (model I) or surface-controlled (model II) model do not
372 fit the limited observations better than using the 5% constant solubility (Figure 6, Ta-
373 ble 1). The soluble Fe and Al depositions from the diffusion-controlled model produce
374 no significantly different dissolved Fe or Al fields from the base run (comparing the ab-
375 solute differences of log-transformed model predictions and observations, not statistically
376 significant at the 0.95 level) except in the Indian Ocean, where the variable solubilities
377 worsen the simulation. The surface-area-controlled soluble iron deposition degrades the
378 dissolved iron comparison in the Indian Ocean and in the global ocean, and improves the
379 north Atlantic simulation (significant at the 0.95 level). The dissolved Al field predicted
380 by the surface-area-controlled solubility model does not significantly change the model-
381 observation comparison in any ocean basin except for the Indian Ocean. The fact that
382 the predicted dissolved Al concentrations fit the data better than Fe suggests that Fe cy-
383 cling in the BEC model also contributes to the discrepancy of simulated to observed iron

384 concentrations. The advantage of using Al as a tracer is that Al cycles similarly to iron
385 but with simpler chemistry and simpler biology. Thus better understanding of Al cycling
386 could serve as foundation for understanding the more complex Fe cycling.

387 The BEC appears to overestimate the surface dissolved iron in the Pacific for all solu-
388 bility scenarios considered here. This overestimate may be caused by poor representation
389 of iron solubility, dust deposition, iron sink processes or some combination of these. In
390 the equatorial north Atlantic, the surface-controlled solubility greatly reduces the overes-
391 timate of dissolved Fe and Al in the base run (though not statistically significant for Al,
392 it can be clearly seen from Figure 6f). The solubility from the surface-controlled model
393 also agrees much better with observations in the North Atlantic than the 5% uniform
394 solubility. Hence the surface-controlled solubility model performs relatively well in the
395 North Atlantic, compared both to other models and to observations. Unfortunately, there
396 are not field observations of solubility in some key regions where the model predictions
397 differ most including the central, equatorial Pacific and parts of the Southern Ocean.

398 We also checked possible ecosystem/biogeochemical impacts of variable iron solubility
399 by comparing other BEC simulated fields among different scenarios and with observations,
400 e.g., surface nitrate, phosphate and silicate concentrations, surface chlorophyll, total bi-
401 ological carbon export at 103 m, total N fixation. However, though all of these fields
402 vary more or less at basin scale with different soluble iron inputs, none of them shows
403 significant change globally. Since the spatial impacts of increasing soluble iron have been
404 discussed in *Krishnamurthy et al.* [2009] using the same ecosystem model, we will not
405 discuss this in detail here.

4. Discussion

406 We explored two plausible relations between trace metal (i.e., Fe and Al) solubility and
407 particle size and transport time. We developed these relations into diffusion-controlled and
408 surface-controlled models to predict the fraction of soluble iron in dust particles. These
409 conceptual models make numerous assumptions to simplify the complex and poorly under-
410 stood dissolution processes on scales relevant to and tractable by present day general cir-
411 culation models. These models neglect many important features such as spatio-temporal
412 variations of particle physical and chemical properties (except size), diurnal and daily
413 variations in aerosol and pH, and cloud processing effects. Both models contain at least
414 one parameter whose measured values range over several orders of magnitude, i.e., the
415 diffusion coefficient for the diffusion-controlled model and the specified reaction rate and
416 the surface roughness factor for the surface-area controlled model. In all cases we picked
417 parameter values to yield reasonable results at the global scale but other combinations
418 of parameter choices are just as valid (and arbitrary). In reality these parameters are
419 not fundamentally constant but are rather functions of trace species, mineralogy, other
420 physical and chemical properties of dust particles and environmental conditions during
421 transport. We neglected this complexity and picked a single value or single relationship
422 constrained by one group of observed solubility data. Although the resulting models
423 produce solubilities in a reasonable range compared to independent measurement, these
424 simplifications tend to eliminate natural variability, and help explain why the models do
425 not predict the full range of observed solubility variations, particularly in the Pacific. From
426 this initial study we can conclude that the two simplified aerosol models we examine are
427 insufficient to remediate the biases between our model and the available observations and

428 that chemical processing is likely playing a predominant role. In determining solubility,
429 we have neglected and simplified processes including dust mineralogy, acidity buffering by
430 neutralizing compounds such as ammonium, solution activity, and photochemistry. More
431 complete and realistic physical-chemical models of solubility in conjunction with more
432 complete atmospheric chemistry may well improve simulations of particle solubility and
433 its evolution.

434 Dust age at deposition is an important variable in both conceptual models. Smaller
435 particles are usually older at deposition and therefore endure more atmospheric processing.
436 Hence dust age at deposition reinforces the effects of particle size. Weather (wind and
437 precipitation) during transport has significant impact on dust age, especially for smaller
438 dust particles.

439 More solubility observations would better constrain and improve our understanding of
440 trace metal solubility. The current observations use different techniques that are not fully
441 comparable with each other. These observations are geographically clustered, mostly in
442 the North Pacific and the North Atlantic. There are few aerosol solubility measurements
443 in the Southern Ocean, where the bio-available iron input is vital [*Krishnamurthy et al.*,
444 2010] and where our models diverge the most from each other and from previous studies.
445 There are no lengthy, continual, much less climatological time series of solubility over land
446 or oceans. In our conceptual models, all the variables including dust deposition, dust age,
447 pH distribution change seasonally. Seasonal cycles of solubility at some fixed locations
448 would thus provide very useful constraints on our models. Considering the difficulties
449 and cost of sampling over open oceans, aerosol solubility measurements over continental
450 regions, especially downwind of dust or pollution sources, would also be very useful.

451 **Acknowledgments.** This research was supported by NSF OCE-0452972, NSF ARC-
452 0714088, NASA NNX07AR23G and NSF OCE-0928204. We thank Alex Baker for sharing
453 data with us. We also thank J. Randerson, N. Mahowald, C. Luo and the anonymous
454 reviewer for suggestions to improve the model and helpful comments.

References

- 455 Ahum, M., and L. Lavkulich (1998), Speciation and solubility relationships of Al, Cu and
456 Fe in solutions associated with sulfuric acid leached mine waste rock, *Environmental*
457 *Geology*, *38*(1), 59–68.
- 458 Anbeek, C. (1992), Surface roughness of minerals and implications for dissolution studies,
459 *Geochim. Cosmochimi. Ac.*, *56*, 1461–1469.
- 460 Anderson, J. R., P. R. Buseck, T. L. Patterson, and R. Arimoto (1996), Characterization
461 of the Bermuda tropospheric aerosol by combined individual-particle and bulk-aerosol
462 analysis, *Atmos. Environ.*, *30*(2), 319–338.
- 463 Arimoto, R., R. A. Duce, B. J. Ray, and U. Tomza (2003), Dry deposition of
464 trace elements to the western North Atlantic, *Global Biogeochem. Cy.*, *17*(1), doi:
465 10.1029/2001GB001406.
- 466 Baker, A. R., and P. L. Croot (2010), Atmospheric and marine controls on aerosol iron
467 solubility in seawater, *Marine Chemistry*, *120*, 4–13.
- 468 Baker, A. R., and T. D. Jickells (2006), Mineral particle size as a control on aerosol iron
469 solubility, *Geophys. Res. Lett.*, *33*, doi:10.1029/2006GL026557.
- 470 Baker, A. R., S. D. Kelly, K. F. Biswas, M. Witt, and T. D. Jickells (2003), Atmo-
471 spheric deposition of nutrients to the Atlantic Ocean, *Geophys. Res. Lett.*, *30*(24),

- 472 doi:10.1029/2003GL018518.
- 473 Behrenfeld, M. J., A. J. Bale, Z. S. Kolber, J. Aiken, and P. G. Falkowski (1996), Con-
474 firmation of iron limitation of phytoplankton photosynthesis in the equatorial Pacific
475 Ocean, *Nature*, *383*, 508–511.
- 476 Boyd, P. W., et al. (2000), A mesoscale phytoplankton bloom in the polar Southern Ocean
477 stimulated by iron fertilization, *Nature*, *407*, 695–702.
- 478 Brantley, S. L. (2008), Kinetics of mineral dissolution, in *Kinetics of water-rock interac-*
479 *tion*, edited by S. L. Brantley, J. D. Kubicki, and A. F. White, pp. 151–210, Springer
480 Science+Business Media, LLC.
- 481 Brantley, S. L., S. Ruebush, J.-H. Jang, and M. Tien (2006), Analysis of (bio)geochemical
482 kinetics of Fe(III) oxides, in *Methods of investigating microbial-mineral interactions*,
483 edited by P. A. Maurice and L. A. Warren, CMS workshop lectures, Vol. 14, The clay
484 mineral society.
- 485 Brunauer, S., P. H. Emmett, and E. Teller (1938), Adsorption of gases in multimolecular
486 layers, *J. Am. Chem. Soc.*, *60*, 309–319.
- 487 Buck, C. S., W. M. Landing, J. A. Resing, and G. T. Lebon (2006), Aerosol iron and
488 aluminum solubility in the northwest Pacific Ocean: Results from the 2002 IOC cruise,
489 *Geochemistry geophysics geosystems*, *7*(4), Q04M07,, doi:10.1029/2005GC000977.
- 490 Buck, C. S., W. M. Landing, and J. A. Resing (2008a), Particle size and aerosol
491 iron solubility: A high-resolution analysis of Atlantic aerosols, *Mar. Chem.*, doi:
492 10.1016/j.marchem.2008.11.002.
- 493 Buck, C. S., W. M. Landing, J. A. Resing, and C. I. Measures (2008b), The solubility
494 and deposition of aerosol Fe and other trace elements in the North Atlantic Ocean:

- 495 Observations from the A16N CLIVAR/CO₂ repeat hydrography section, *Mar. Chem.*,
496 doi:10.1016/j.marchem.2008.08.003.
- 497 Cheah, S.-F., S. M. Kraemer, J. Cervini-Silva, and G. Sposito (2003), Steady-state
498 dissolution kinetics of goethite in the presence of desferrioxamine B and oxalate lig-
499 ands: implications for the microbial acquisition of iron, *Chem. Geol.*, *198*, 63–75, doi:
500 10.1016/S0009-2541(02)00421-7.
- 501 Chen, Y., and R. L. Siefert (2004), Seasonal and spatial distributions of atmospheric total
502 and labile iron over the tropical and subtropical North Atlantic Ocean, *J. Geophys. Res.*,
503 *109*, doi:10.1029/2003JD003958.
- 504 Chuang, P. Y., R. M. Duvall, M. M. Shafer, and J. J. Schauer (2005), The origin of
505 water soluble particulate iron in the Asian atmospheric outflow, *Geophys. Res. Lett.*,
506 *32*, doi:10.1029/2004GL021946.
- 507 Claquin, T., M. Schulz, and Y. J. Balkanski (1999), Modeling the mineralogy of atmo-
508 spheric dust sources, *J. Geophys. Res.*, *104*(D18), 22,243–22,256.
- 509 Collins, W. D., et al. (2006), The community climate system model version3 (CCSM3),
510 *J. Climate*, *19*(11), 2122–2161.
- 511 Cwiertny, D. M., J. Baltrusaitis, G. J. Hunter, A. Laskin, M. M. Scherer, and V. H. Gras-
512 sian (2008), Characterization and acid-mobilization study of iron-containing mineral
513 dust source materials, *J. Geophys. Res.*, *113*, doi:10.1029/2007JD009332.
- 514 Desboeufs, K. V., R. Losno, and Colin (2003), Relationship between droplet pH and
515 aerosol dissolution kinetics: Effect of incorporated aerosol particles on droplet pH during
516 cloud processing, *J. Atmos. Chem.*, *46*, 159–172.

- 517 Doney, S. C., K. Lindsay, and J. K. Moore (2003), Global ocean carbon cycle modeling,
518 in: Ocean biogeochemistry: a JGOFS synthesis, *Ed. M. Fasham, Springer-Verlag*, pp.
519 217–238.
- 520 Fan, S.-M., W. J. Moxim, and H. L. II (2006), Aeolian input of bioavailable iron to the
521 oceans, *Geophys. Res. Lett.*, *33*(L07602), doi:10.1029/2005GL024852.
- 522 Fung, I. Y., S. K. Meyna, I. Tegen, S. C. Doney, J. G. John, and J. K. B. Bishop (2000),
523 Iron supply and demand in upper ocean, *Global Biogeochem. Cy.*, *14*(1), 281–295.
- 524 Grassian, V. H. (2001), Heterogeneous uptake and reaction of nitrogen oxides and volatile
525 organic compounds on the surface of atmospheric particles including oxides, carbon-
526 ates, soot and mineral dust: implications for the chemical balance of the troposphere,
527 *Int. Rev. Phys. Chem.*, *20*(3), 467–548.
- 528 Han, Q., and C. S. Zender (2010), Desert dust aerosol age characterized by Mass-Age
529 Tracking (MAT) of tracers, *J. Geophys. Res.*, *115*, doi:10.1029/2010JD014155.
- 530 Han, Q., J. K. Moore, C. Zender, C. Measures, and D. Hydes (2008), Constraining
531 oceanic dust deposition using surface ocean dissolved Al, *Global Biogeochem. Cy.*, *22*,
532 doi:10.1029/2007GB002975.
- 533 Hand, J. L., N. M. Mahowald, Y. Chen, R. L. Siefert, C. Luo, A. Subramaniam, and
534 I. Fung (2004), Estimates of atmospheric-processed soluble iron from observations and
535 a global mineral aerosol model: Biogeochemical implications, *J. Geophys. Res.*, *109*,
536 doi:10.1029/2004JD004574.
- 537 Hänel, G. (1976), The properties of atmospheric aerosol particles as functions of the
538 relative humidity at thermodynamic equilibrium with the surrounding moist air.

539 Jickells, T., T. Church, A. Veron, and R. Arimoto (1994), Atmospheric inputs of man-
540 ganese and aluminium to the Sargasso Sea and their relation to surface water concen-
541 trations, *Mar. Chem.*, *46*, 283–292.

542 Jickells, T. D., and L. J. Spokes (2001), Atmospheric iron inputs to the oceans, in *The*
543 *biogeochemistry of iron in seawater*, edited by D. R. Turner and K. A. Hunter, pp.
544 85–121, John Wiley & Sons Ltd.

545 Jickells, T. D., et al. (2005), Global iron connections between desert dust, ocean biogeo-
546 chemistry and climate, *Science*, *308*(67), doi:10.1126/science.1105959.

547 Johansen, A. M., and J. M. Key (2006), Photoreductive dissolution of ferrihydrite by
548 methanesulfinic acid: Evidence of a direct link between dimethylsulfide and iron-
549 bioavailability, *Geophys. Res. Lett.*, *33*.

550 Johansen, A. M., R. L. Siefert, and M. R. Hoffmann (2000), Chemical composition of
551 aerosols collected over the tropical North Atlantic Ocean, *J. Geophys. Res.*, *105*(D12),
552 15,277–15,312.

553 Journet, E., K. V. Desboeufs, S. Caquineau, and J.-L. Colin (2008), Mineralogy as a crit-
554 ical factor of dust iron solubility, *Geophys. Res. Lett.*, *35*, doi:10.1029/2007GL031589.

555 Krishnamurthy, A., J. K. Moore, N. Mahowald, C. Luo, S. C. Doney, K. Lindsay,
556 and C. S. Zender (2009), Impacts of increasing anthropogenic soluble iron and nitro-
557 gen deposition on ocean biogeochemistry, *Global Biogeochem. Cy.*, *23*(GB3016), doi:
558 10.1029/2008GB003440.

559 Krishnamurthy, A., J. K. Moore, N. Mahowald, C. Luo, and C. S. Zender (2010), Im-
560 pacts of atmospheric nutrient inputs on marine biogeochemistry, *J. Geophys. Res.*,
561 *115*(G01006), doi:10.1029/2009JG001115.

- 562 Lafon, S., I. N. Sokolik, J. L. Rajot, S. Caquineau, and A. Gaudichet (2006), Charac-
563 terization of iron oxides in mineral dust aerosols: Implications for light absorption,
564 *J. Geophys. Res.*, *111*(D21207), doi:10.1029/2005JD007016.
- 565 Luo, C., N. M. Mahowald, N. Meskhidze, Y. Chen, R. L. Siefert, A. R. Baker, and A. M.
566 Johansen (2005), Estimation of iron solubility from observations and a global aerosol
567 model, *J. Geophys. Res.*, *110*, D23307, doi:10.1029/2005JD006059.
- 568 Luo, C., C. S. Zender, H. Bian, and S. Metzgerc (2007), Role of ammonia chemistry and
569 coarse mode aerosols in global climatological inorganic aerosol distributions, *Atmos. En-*
570 *viron.*, *41*, 2510–2533, doi:10.1016/j.atmosenv.2006.11.030.
- 571 Luo, C., N. Mahowald, T. Bond, P. Y. Chuang, P. Artaxo, R. Siefert, Y. Chen,
572 and J. Schauer (2008), Combustion iron distribution and deposition, *Global Bio-*
573 *geochem. Cy.*, *22*, doi:10.1029/2007GB002964.
- 574 Mahowald, N. M., P. J. Rasch, B. E. Eaton, S. Whittlestone, and R. G. Prinn (1997),
575 Transport of (222)radon to the remote troposphere using the model of atmospheric
576 transport and chemistry and assimilated winds from ECMWF and the National Center
577 for Environmental Prediction NCAR, *J. Geophys. Res.*, *102*(D23), 28,139–28,151.
- 578 Mahowald, N. M., A. R. Baker, G. Bergametti, N. Brooks, R. A. Duce, T. D. Jickells,
579 N. Kubilay, J. M. Prospero, and I. Tegen (2005), Atmospheric global dust cycle and
580 iron inputs to the ocean, *Global Biogeochem. Cy.*, *19*, doi:10.1029/2004GB002402.
- 581 Mahowald, N. M., et al. (2009), Atmospheric iron deposition: Global distribu-
582 tion, variability, and human perturbations, *Annu. Rev. Mar. Sci.*, *1*, 245–278, doi:
583 10.1146/annurev.marine.010908.163727.

- 584 Martin, H. B., and S. E. Fitzwater (1988), Iron deficiency limits phytoplankton growth in
585 the north-east Pacific subarctic, *Nature*, *331*, 341–343.
- 586 Measures, C. I., and S. Vink (2000), On the use of dissolved aluminum in surface waters
587 to estimate dust deposition to ocean, *Global Biogeochem. Cy.*, *14*(1), 317–327.
- 588 Measures, C. I., T. Sato, S.Vink, S. Howell, and Y. H. Li (2010), The fractional solubility
589 of aluminium from mineral aerosols collected in Hawaii and implications for atmospheric
590 deposition of biogeochemically important trace elements, *Marine Chemistry*, *120*, 144–
591 153.
- 592 Moore, J. K., and O. Braucher (2008), Sedimentary and mineral dust sources of dissolved
593 iron to the world ocean, *Biogeosciences*, *5*, 631–656.
- 594 Moore, J. K., S. C. Doney, J. A. Kleypas, D. M. Glover, and I. Y. Fung (2002), An interme-
595 diate complexity marine ecosystem model for the global domain, *Deep-Sea Res. Pt. II*,
596 *49*, 403–462.
- 597 Moore, J. K., S. C. Doney, and K. Lindsay (2004), Upper ocean ecosystem dynamics and
598 iron cycling in a global three-dimensional model, *Global Biogeochem. Cy.*, *18*, GB4028,
599 doi:10.1029/2004GB002220.
- 600 Prospero, J. M., R. T. Nees, and M. Uematsu (1987), Deposition rate of particulate
601 and dissolved aluminum derived from saharan dust in precipitation at miami, florida,
602 *J. Geophys. Res.*, *92*, 14,723–14,731.
- 603 Sarthou, G., et al. (2003), Atmospheric iron deposition and sea-surface dissolved iron
604 concentrations in the eastern Atlantic Ocean, *Deep-Sea Res. Pt. I*, *50*, 1339–1352, doi:
605 10.1016/S0967-0637(03)00126-2.

- 606 Sato, T. (2003), The fractional solubility of aluminum from atmospheric aerosols, Master's
607 thesis, University of Hawaii at Manoa, Honolulu, HI, USA.
- 608 Seinfeld, J. H., and S. N. Pandis (2006), *Atmospheric chemistry and physics*, second ed.,
609 John Wiley, Hoboken, N. J.
- 610 Shi, Z., M. D. Krom, S. Bonneville, A. R. Baker, T. D. Jickells, and L. G. Benning (2009),
611 Formation of iron nanoparticles and increase in iron reactivity in mineral dust during
612 simulated cloud processing, *Environ. Sci. Technol.*, *43*, 6592–6596.
- 613 Shi, Z., S. Bonneville, M. D. Krom, K. S. Carslaw, T. D. Jickells, A. R. Baker, and L. G.
614 Benning (2011), Iron dissolution kinetics of mineral dust at low pH during simulated
615 atmospheric processing, *Atmos. Chem. Phys.*, doi:10.5194/acp-11-995-2011.
- 616 Shi, Z., et al. (2010), Influence of chemical weathering and aging of iron oxides on
617 the potential iron solubility of Saharan dust during simulated atmospheric processing,
618 *Global Biogeochem. Cy.*, *25*, doi:10.1029/2010GB003837.
- 619 Sholkovitz, E. R., P. N. Sedwick, and T. M. Church (2009), Influence of anthropogenic
620 combustion emissions on the deposition of soluble aerosol iron to the ocean: Empirical
621 estimates for island sites in the North Atlantic, *Geochim. Cosmochimi. Ac.*, *73*, 3981–
622 4003.
- 623 Siefert, R. L., S. O. Pehkonen, Y. Erel, and M. R. Hoffmann (1994), Iron photochemistry
624 of aqueous suspensions of ambient aerosol with added organic-acids, *Geochim. Cos-
625 mochimi. Ac.*, *58*(15), 3271–3279.
- 626 Siefert, R. L., A. M. Johansen, and M. R. Hoffmann (1999), Chemical characterization
627 of ambient aerosol collected during the southwest monsoon and intermonsoon seasons
628 over the Arabian Sea: Labile-Fe(II) and other trace metals, *J. Geophys. Res.*, *104*,

- 629 3511–3526.
- 630 Sposito, G. (1996), *The environmental chemistry of aluminum*, second ed., CRC Press.
- 631 Stumm, W. (1992), *Chemistry of the solid-water interface*, John Wiley & Sons, Inc.
- 632 Sullivan, P. J., K. J. Reddy, and J. L. Yelton (1988), Solubility relationships of aluminum
633 and iron minerals associated with acid mine drainage, *Environmental Geological Water
634 Science*, *11*(3), 283–287.
- 635 Taylor, S. R., and S. M. McLennan (1985), *The continental crust: its composition and
636 evolution*, Blackwells, Oxford, England.
- 637 Watson, E. B., and E. F. Baxter (2007), Diffusion in solid-Earth systems,
638 *Earth Planet. Sc. Lett.*, *253*, 307–327, doi:10.1016/j.epsl.2006.11.015.
- 639 Wedepohl, K. H. (1995), The composition of the continental crust, *Geochim. Cos-
640 mochimi. Ac.*, *59*(7), 1217–1232.
- 641 Wehrli, B., E. Wieland, and G. Furrer (1990), Chemical mechanisms in the dissolution
642 kinetics of minerals: the aspect of active sites, *Aquat. Sci.*, *52*(1), 3–31.
- 643 White, A. F., A. E. Blum, M. S. Schulz, T. D. Bullen, J. W. Harden, and M. L. Peterson
644 (1996), Chemical weathering rates of a soil chronosequence on granitic alluvium: i.
645 quantification of mineralogical and surface area changes and calculation of primary
646 silicate reaction rates, *Geochim. Cosmochimi. Ac.*, *60*(14), 2533–2550.
- 647 Zender, C. S., H. Bian, and D. Newman (2003), Mineral Dust Entrainment and Deposition
648 (DEAD) model: Description and 1990s dust climatology, *J. Geophys. Res.*, *108*(D14),
649 doi:10.1029/2002JD002775.
- 650 Zhu, X., J. M. Prospero, F. J. Millero, D. L. Savoie, and G. W. Brass (1992), The
651 solubility of ferric ion in marine mineral aerosol solutions at ambient relative humidities,

652 *Mar. Chem.*, 38, 91–107.

653 Zhuang, G., Z. Yi, R. A. Duce, and P. R. Brown (1992), Link between iron and sulphur
654 cycles suggested by detection of Fe(II) in remote marine aerosols, *Nature*, 355.

655 Zuo, Y., and J. Holgné (1992), Formation of hydrogen peroxide and depletion of oxalic acid
656 in atmospheric water by photolysis of iron(III)-oxalato complexes, *Environ. Sci. Tech-*
657 *nol.*, 26, 1014–1022.

Table 1: Iron deposition, solubility and ecosystem responses in different ocean basins

Basins	Total Fe Soluble Fe (Tg/yr)		Solubility (%) of Fe and Al		RMSD ^d of dissolved Fe (nM)		RMSD of dissolved Al (nM)					
	5% ^a	I ^b	II ^c	I	II	5%	I	II				
Pacific	1.24	0.062	0.082	0.124	6.6	10.1	0.501	0.514	0.616	0.529	0.476	0.601
North Atlantic	5.70	0.285	0.256	0.224	4.5	3.8	0.353	0.347	0.300	0.350	0.335	0.305
South Atlantic	0.51	0.025	0.029	0.035	5.6	7.0	0.527	0.523	0.587	0.320	0.313	0.301
Indian Ocean	1.23	0.062	0.048	0.050	3.9	4.0	0.256	0.362	0.388	0.278	0.351	0.380
Southern Ocean	1.34	0.067	0.042	0.010	3.1	0.7	0.462	0.482	0.452	0.263	0.349	0.325
Mediterranean Sea	0.53	0.026	0.010	0.015	1.8	2.8	NA	NA	NA	0.167	0.148	0.128
Oceans total ^e	11.41	0.570	0.481	0.470	4.2	4.1	0.445	0.465	0.505	0.352	0.349	0.357
Global total	50.68	2.534	0.979	0.904	1.9	1.8	NA	NA	NA	NA	NA	NA

^a Globally uniform 5% solubility assumption^b Diffusion-controlled model^c Surface-controlled model^d Root mean square difference, after logarithm transformation^e Ocean total also include dust deposition in marginal seas.

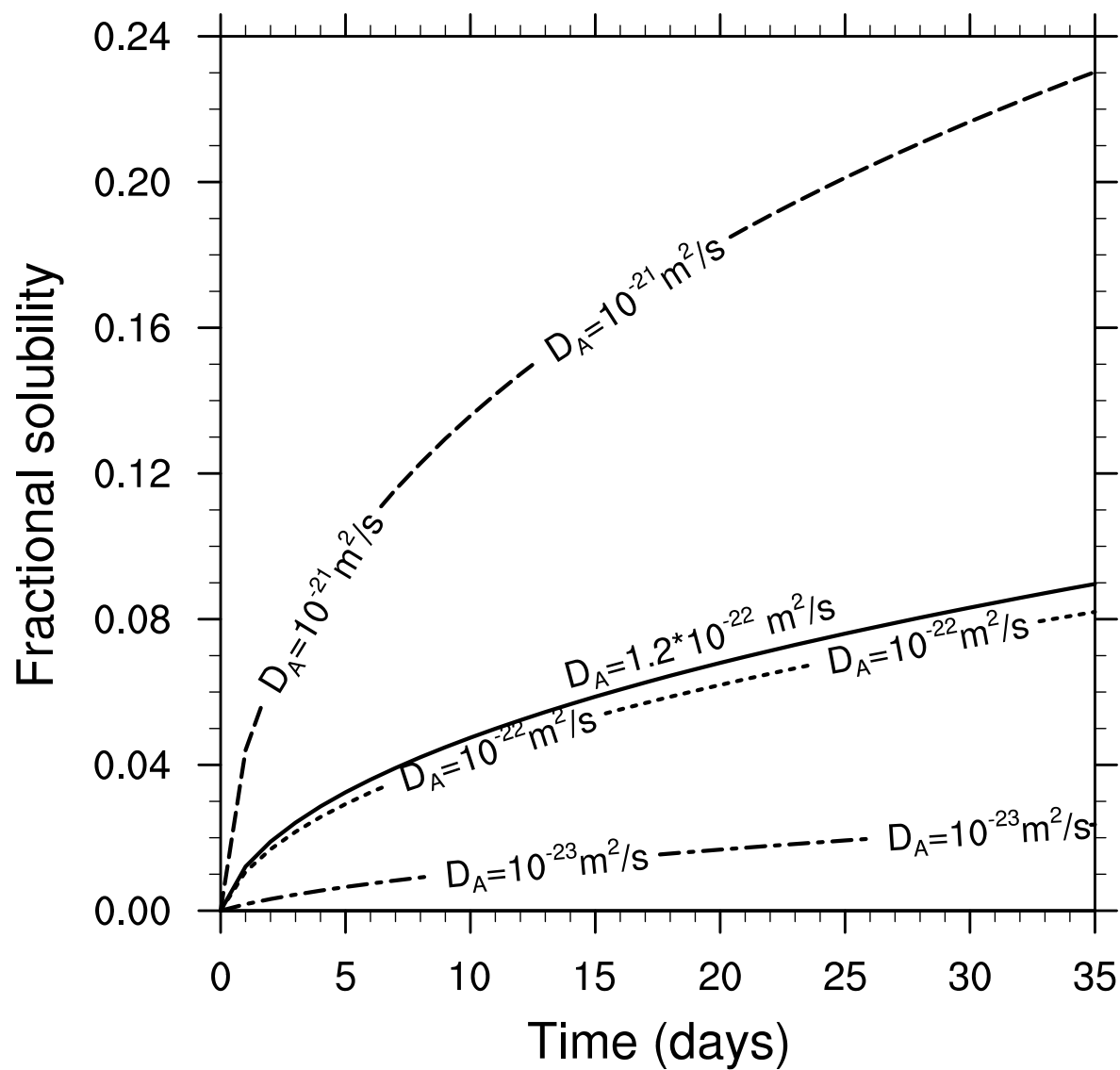


Figure 1: Evolution of fractional solubility S as a function of diffusion coefficient D_A in diffusion-controlled model.

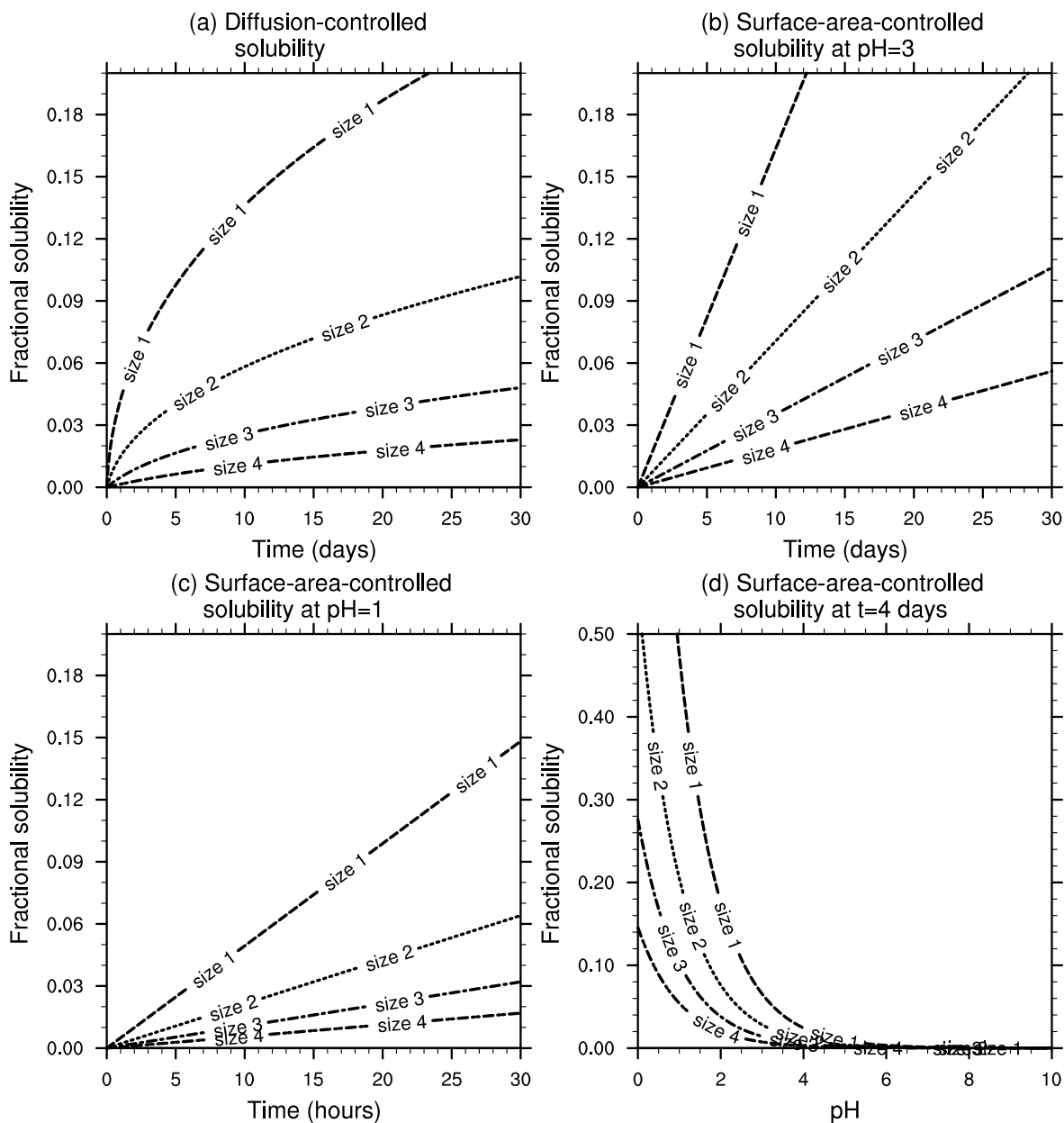


Figure 2: Fractional solubility for different size bins from (a) diffusion-controlled model in a 30-day period, (b) surface-controlled model at $\text{pH} = 3$ in a 30-day period, (c) surface-controlled model at $\text{pH} = 1$ in a 30-hour period, (d) surface-controlled model at $t = 4$ days at different pH conditions.

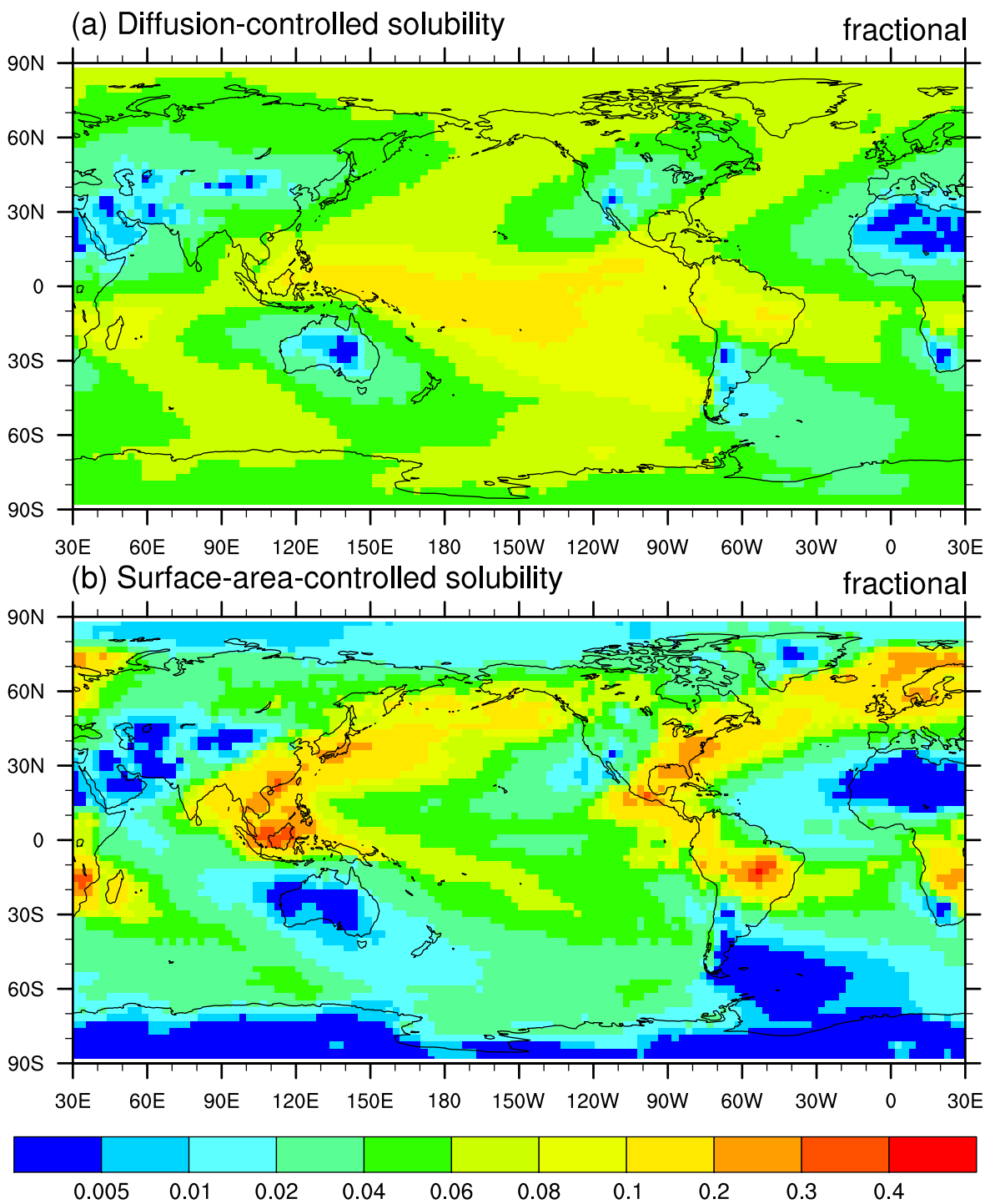


Figure 3: Geographic solubility distributions from: (a) diffusion-controlled model, (b) surface-area-controlled model.

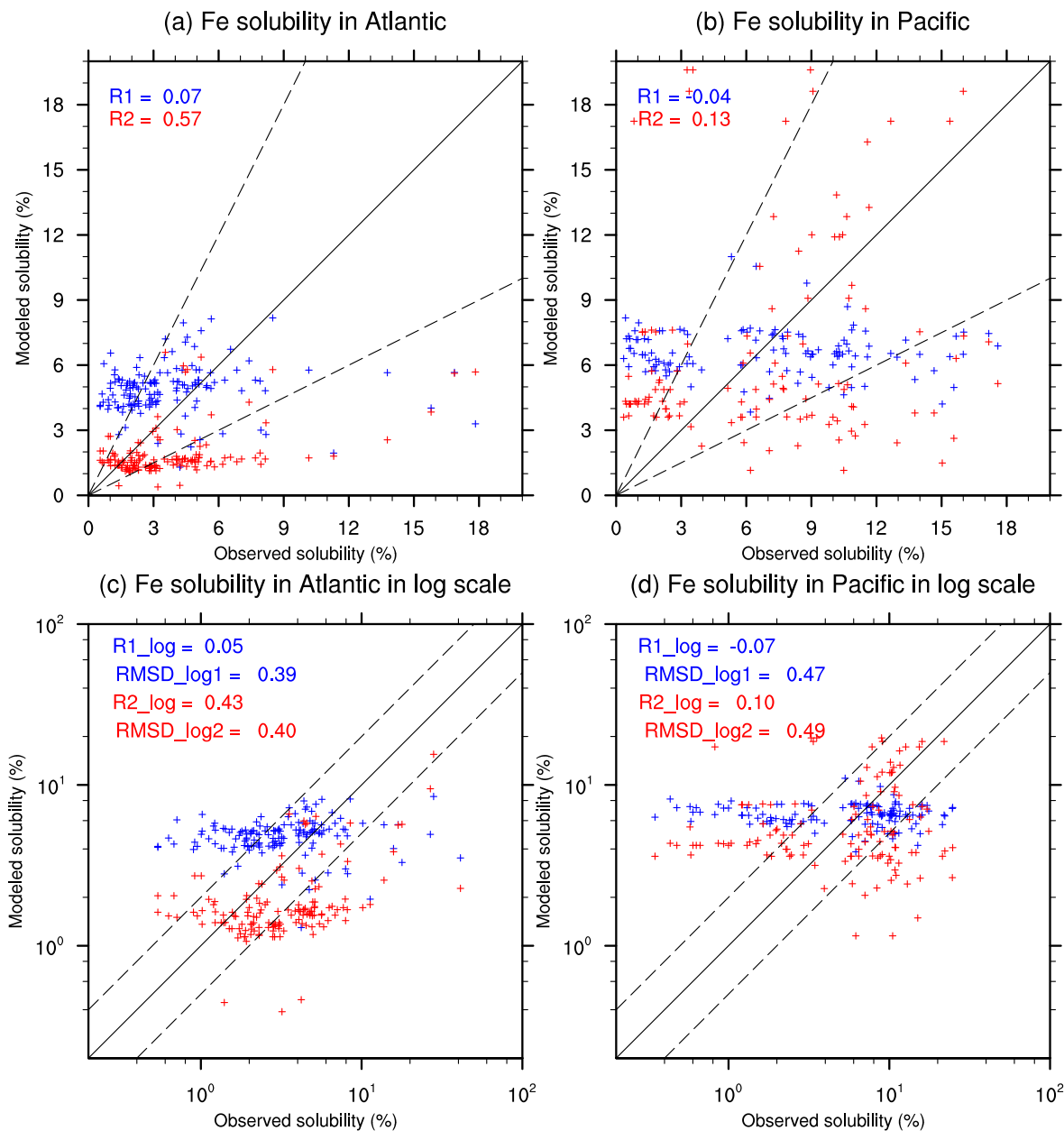


Figure 4: Fe solubilities predicted by diffusion-controlled (blue) and surface-area-controlled (red) models compared to observations (a) in the Atlantic from cruises MP01-MP09, JCR and M55, (b) in the Pacific from cruises MP01-MP09, (c) Atlantic Ocean on log scale, (d) Pacific Ocean on log scale. Dashed lines represent factor of two agreement. RMSD is root mean square difference after logarithmic transformation.

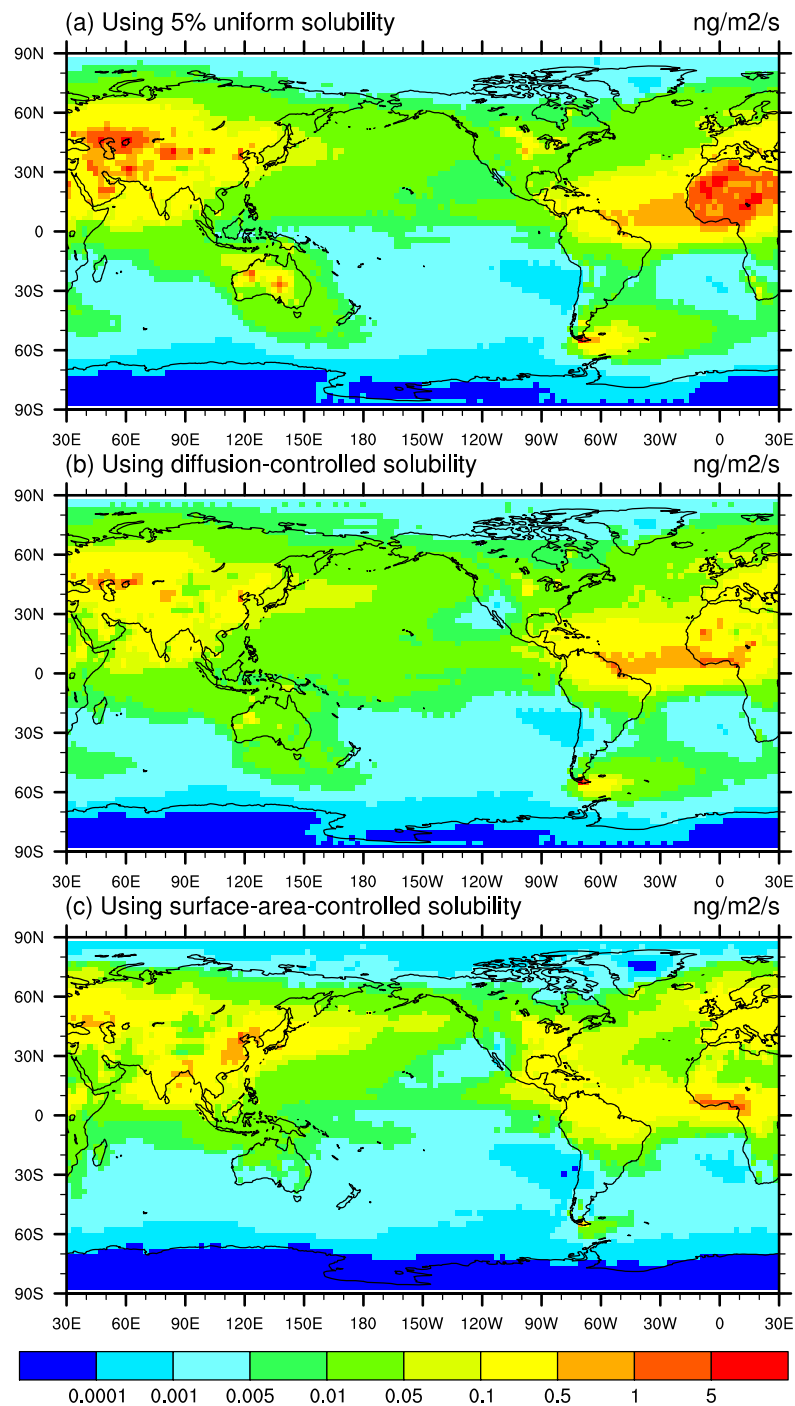


Figure 5: Modeled soluble iron deposition from (a) 5% global uniform solubility, (b) solubility predicted by diffusion-controlled conceptual model, (c) solubility predicted by surface-controlled conceptual model. Dust field is simulated by DEAD using the 1990-1999 climatology [Zender *et al.*, 2003] and the iron content of the dust is 3.5% by weight.

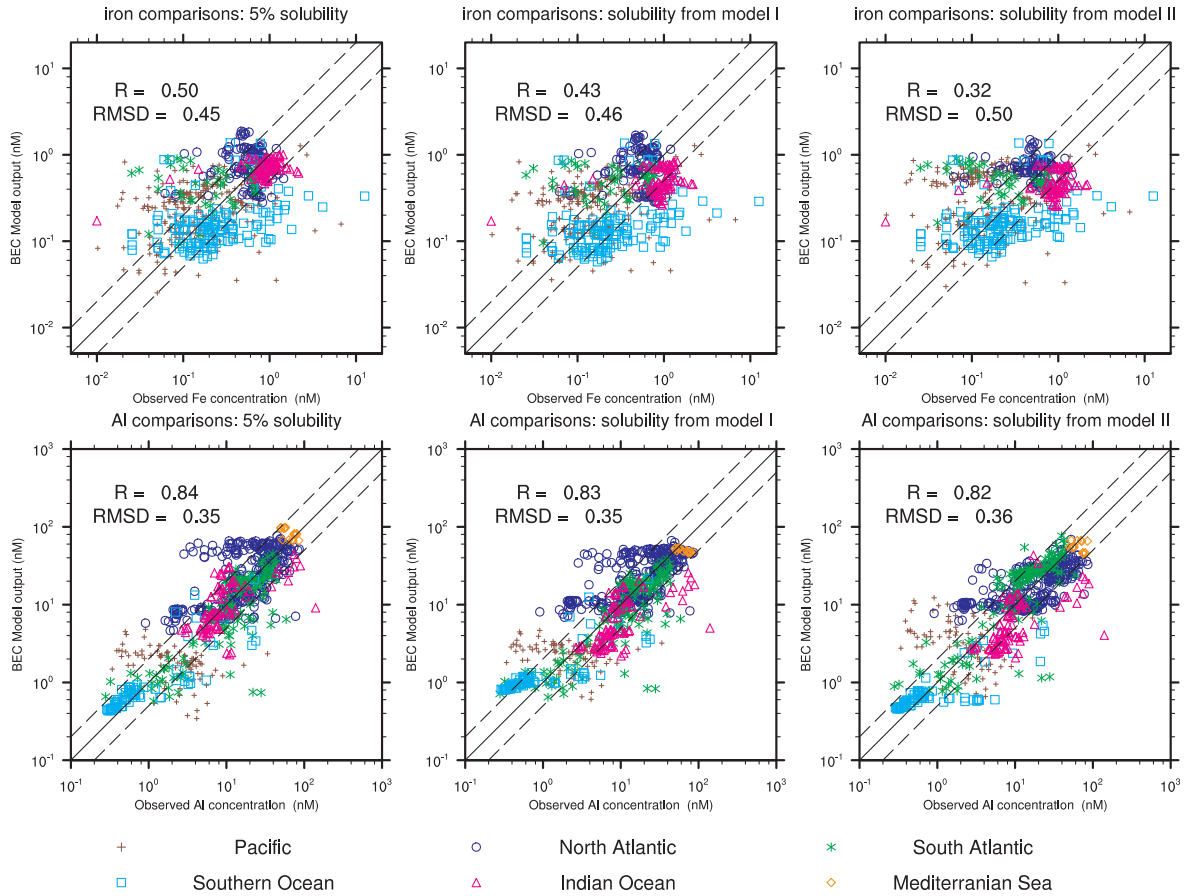


Figure 6: Dissolved Fe and Al concentrations predicted by the BEC models with different solubility fields compared to observations.